

## ANALYZING ANTIMICROBIAL ACTIVITY OF ALUMINIUM DOPED ZnO THIN FILMS

BA. Anandh<sup>1,✉</sup>, R. Sakthivel<sup>1</sup>, A. Shankar Ganesh<sup>1</sup>, S. Subramani<sup>1</sup>  
and A.T. Rajamanickam<sup>2</sup>

<sup>1</sup>Department of Electronics, PSG College of Arts & Science, Coimbatore -641014,  
Tamil Nadu, India

<sup>2</sup>Department of Electronics, Sri Ramakrishna Mission Vidyalaya College of Arts and Science,  
Coimbatore-641020, Tamil Nadu, India

✉Corresponding Author: [anandh.ba@gmail.com](mailto:anandh.ba@gmail.com)

### ABSTRACT

The two-step SILAR approach was used to create pure and Aluminium (Al) doped Zinc Oxide (ZnO) thin films. The structural, optical, and morphological properties of pure ZnO thin film and ZnO thin films doped with Al (1, 3, and 5)% were investigated. All the sample's diffraction peaks were mapped to a hexagonal Wurtzite form. For the synthesized thin films, dislocation density, crystallite size, microstrain, and lattice parameters were calculated. Pure ZnO thin films have a spherical structure, while Al-doped ZnO thin films have a hexagonal-faced rod-like shape. The bandgap of the prepared thin film reduces with the rise in Al content. The occurrence of deep level and near band edge emissions were confirmed by photoluminescence (PL) investigations. The maximal zone of inhibition was studied using the Agar diffusion process on Gram-positive and Gram-negative (i.e., *S.aureus* and *E.coli*) bacteria. Pure and Al-doped ZnO both showed significant antibacterial activity. All the samples exhibit significant antimicrobial activity.

**Keywords:** Al-doped ZnO, XRD, FESEM, UV-Vis, Antimicrobial Activity.

RASĀYAN *J. Chem.*, Vol. 15, No.1, 2022

### INTRODUCTION

Zinc oxide is a semiconductor with an extensive range of potential uses due to its unique physical features. The hexagonal wurtzite form of ZnO is much more stable at room temperature than other forms like rock salt and zinc blend.<sup>1</sup> Thin film research has improved several novel aspects of analysis that are based on unique characteristics and structures. At room temperature, ZnO has excellent thermal stability, higher chemical stability and a broad bandgap (3.37eV). Thin films made of ZnO have high electrical resistivity, outstanding optical, electrical properties, less price, and non-toxicity.<sup>2</sup> ZnO, an inorganic substance, has a high resistivity against microbes.<sup>3</sup> ZnO is a significant substance for preventing food microorganisms like *Staphylococcus aureus* (*S.aureus*) and *Escherichia coli* (*E.coli*) from contaminating foodstuff.<sup>4</sup> It can also be found in skin-care items such as creams, baby powder, and diaper rashes discovered that ZnO has strong antifungal action and is utilized to protect wood against fungal activity.<sup>5,6</sup> Chemisorptions and adsorption alter the surface conductivity of pure ZnO films, making them unstable.<sup>7</sup> Sn, Cu, Ag, Mn, Mg, Al, and Fe are anionic and cationic dopants that can affect the characteristics of Zinc Oxide and make thin films more conductive, which may be another alternative for lower cost transparent conductive films for an application like antimicrobial, gas detecting, solar cells, and photocatalytic properties, etc.,<sup>8-11</sup> Aluminium is one of the finest doping material for producing the thin film that is conductive and transparent in the visible spectrum. As a result, it is suitable for transparent conductive composites. Successive Ionic Layer Adsorption and Reaction (SILAR), Sputtering, Dip coating, sol-gel deposition, spray pyrolysis, chemical bath deposition are some of the current thin film deposition processes.<sup>12-17</sup> SILAR most often used technique for producing thin films due to its convenience, low cost, nonvacuum nature, and ability to coat on more space. The objective of this research is to use the SILAR technique for making pure ZnO thin films and doping the Aluminium in ZnO thin films and to evaluate their morphological, optical, and structural properties. In addition, the antimicrobial activity of all the prepared samples was examined using Agar diffusion method.

## EXPERIMENTAL

The SILAR technique is utilized to create pure and Al-doped ZnO thin films on glass slides. Pure ZnO thin film is synthesized by using zinc acetate dehydrates (ZAD) as the source material. In 100ml of ethanol (solvent) 0.1M of the ZAD (precursor) was dissolved and to achieve a clear and homogenous zincate solution, monoethanolamine (MEA) is added dropwise as a stabilizing agent. Al-doped ZnO thin films were synthesized using aluminium acetate as the dopant material. The zincate bath solution is made for (1, 3, and 5) % content of Al dopant and also for pure ZnO. A clean glass substrate was dipped alternately in a zincate (cationic) solution bath at room temperature and hot deionized water (anionic solution) was maintained at 90°C to 100°C for film deposition. A single set of dips consists of 30 seconds in a zincate solution followed by 30 seconds in warm deionized water. This procedure was performed 30 times to get the thin film, and post-annealing was done at 300°C.

### Antibacterial Assessment

The antibacterial action of the prepared samples was tested on *S.aureus* and *E.coli*. The antibacterial action is measured using the agar diffusion method. Within sterile Petri dishes, sterile Muller Hinton (MHA) agar was spread. The cfu/ml concentration of the culture material was adjusted to 10<sup>8</sup>. A sterile cotton swab was used to swab the agar plate's surface. The test samples were placed in the mid of the plates and incubation was done at 37°C for 24 hours. The interrupted growth sample was then evaluated on the incubated plates. Inhibition growth of the test specimen was analyzed.

### Antifungal Assessment

The antifungal action of the prepared samples was studied using the agar diffusion method. Antifungal testing was conducted using *Aspergillus niger* and Potato dextrose agar media. The ready potato dextrose agar medium was supplied with a petri dish and sterile distilled water with a few glass beads was inoculated with fungal spores and energy-shaken so the spores could be suspended. At 1.0 ± 0.1 ml of inoculum, the agar surface was diffused evenly. The testing specimens were placed in the agar plates and incubation was done at 27°C. After the incubation period, the area of mycosis below and on the sides was measured. The growth of inoculums on the incubated plates was checked for interruptions. The width of its clear area was measured to determine the assessment sample's inhibitory effect.

## RESULTS AND DISCUSSION

### Structural Analysis

The XRD peaks of pure and Al-doped ZnO thin films are depicted in Fig.-1 which are post-annealed at 300°C. The hexagonal Wurtzite form of the deposited films is confirmed by the diffraction peaks, which match the 36-1451 JCPDS card. The (002) plane has the strongest intensity, indicating that particulates are aligned along the c-axis. This could be due to surface energy and low internal stress, and the high atomic density that permits crystallites to grow easily along the c-axis.<sup>18</sup> The major peak position has shifted to the right. The doped samples show a shift to the upper angle side in the planes (100), (002), and (101). The feature of the dopant Al<sup>3+</sup> ion's ionic radii, which is tiny compared to the Zn<sup>2+</sup> ion, is responsible for the observed shift in the peak. Peaks were also seen to widen as Al concentration increased.

Table-1: Structural Properties of Pure, Al-doped ZnO Thin Films

Samples	Lattice Constants (Å)		Crystallite Size (D)nm	Micro Strain (ε) x 10 <sup>-3</sup>	Dislocation Density (δ) x 10 <sup>15</sup> lines/m <sup>2</sup>	Unit Cell Volume (Å) <sup>3</sup>
	a	c				
Pure ZnO	3.2492	5.2015	29.91	1.1025	1.2024	47.6139
1 % Al	3.2391	5.1795	19.19	2.6767	1.8753	47.1123
3 % Al	3.2381	5.1754	19.27	2.6783	1.8706	47.0456
5 % Al	3.2406	5.1819	18.32	2.2516	1.9638	47.1342

Table-1 lists the structural properties of prepared thin films. Debye-Scherrer's formula is utilized to compute the crystallite size of the deposited films. Table 1 reveals, that the size of crystallites for Al incorporated

films is smaller in comparison to pure ZnO thin film. This could be due to the stress caused and the high number of dislocations by the ionic radii of Al ions inhabiting interstitial locations inside the lattice of ZnO crystals.<sup>19</sup> The produced films' lattice constants are very much nearer to the standard values. In Al-doped films, the lattice constants are smaller than those in pure films. The microstrain and crystallite size obtained reveal that they are reactive to Aluminium incorporation. Figure-2 depicts the change in microstrain and crystallite size with variation in Al content, indicating a potential reduction in crystallite size as evidenced by the broadening of the diffraction pattern. Pure ZnO film has a dislocation density of 1.2024 lines/m<sup>2</sup>, but following Al doping, it rises to 1.9638 lines/m<sup>2</sup>. These findings show the ZnO thin film doped with Al has a greater level of lattice defect.

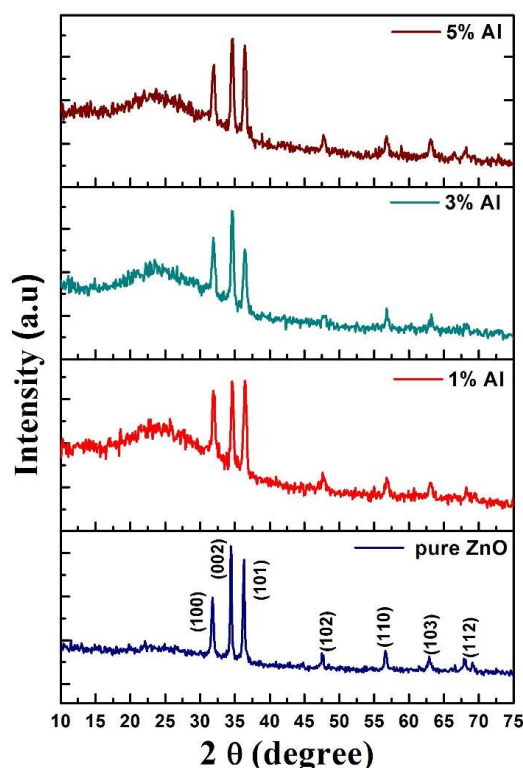


Fig.-1: X-ray Diffraction Pattern

### Surface Morphology

Figure-3 shows pictures of Al-doped and pure ZnO thin films taken with a Field Emission Scanning Electron Microscope (FESEM). It displays sphere shape for pure ZnO thin film. Figure-3 also exhibits doping with Al causes a significant change in grain size, including a transition from a spherical to a hexagonal-faced rod-like structure. The alignment of the grains in ZnO doped with 1% Al is random, but once the content has risen to 3% and 5%, the grains agglomerate and cover the full substrate area with a rod-like morphology. The creation of quantum characteristics on the surface causes such changes in particle shape, as does the reverse effect of Al-O-Zn oxide production.<sup>20</sup> The images clearly show that when the Al content rises, the average crystallite size decreases. As a result, Al doping is thought to have a key role in influencing the morphological aspect of the film.

The Atomic Force Microscopy (AFM) graph is given in Fig.-4 for the thin film of ZnO in pure form and also thin films of ZnO doped with Al with a scan region of 3x3μm. The surface characteristics of the ZnO thin films doped with Al appear to be dense and of excellent standard. Pure ZnO has an even surface, as well as the surface roughness increases considerably as the Al ratio increases. The root mean square (RMS) value of pure ZnO thin film is 10.76 and for (1, 3, and 5) % Al concentrations, the RMS values are 23.87, 34.96, and 44.29. For pure, (1, 3, and 5) % Al ratios, the average roughness is 5.46, 15.99, 26.30, and 32.98. Based on the AFM results, the smoothness of the coated surface reduces as the dopant ratio increases.<sup>21</sup>

The chemical elements of the samples are revealed using EDS and shown was shown in Fig.-5. It shows the existence of Oxygen and Zinc in the ZnO thin film, as well as the inclusion of Al. The Si spike i.e.,

silicon within EDS is caused by the glass substrate. EDS further proves that, when the doping level rises, Al atomic percentage rises from 0.92 to 3.08.

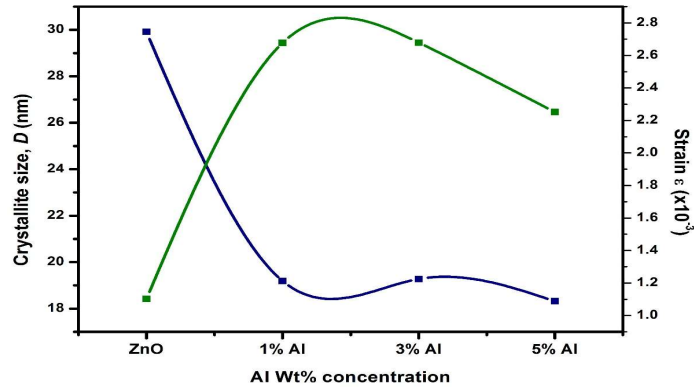


Fig.-2: Microstrain and Crystallite Size of ZnO Thin Films with varying Al Ratio

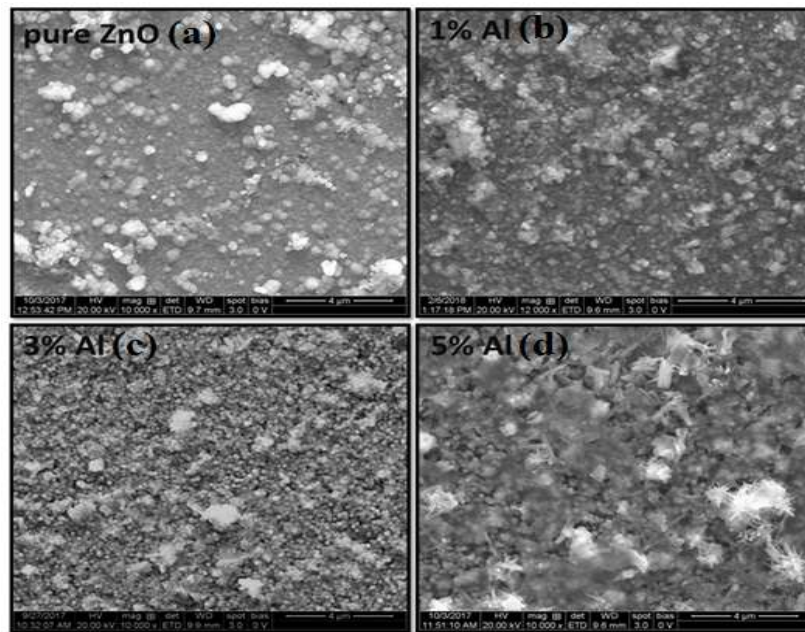


Fig.-3: FESEM Images

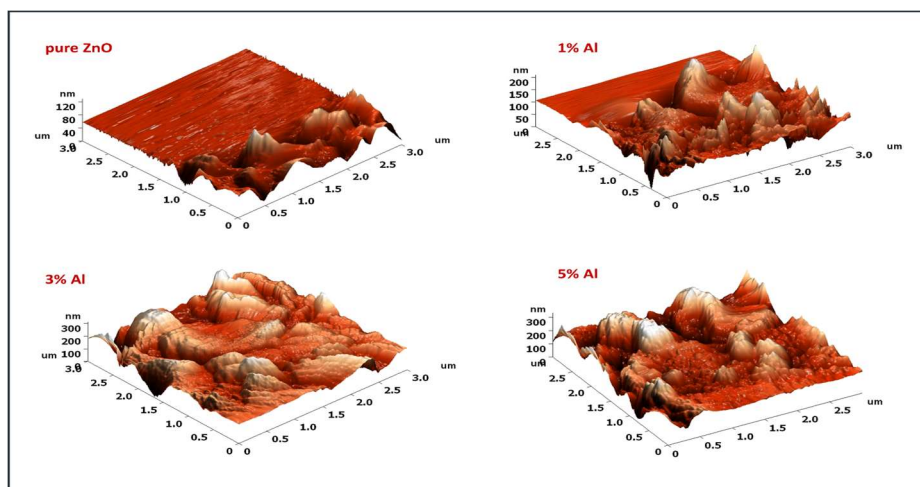


Fig.-4: AFM Images

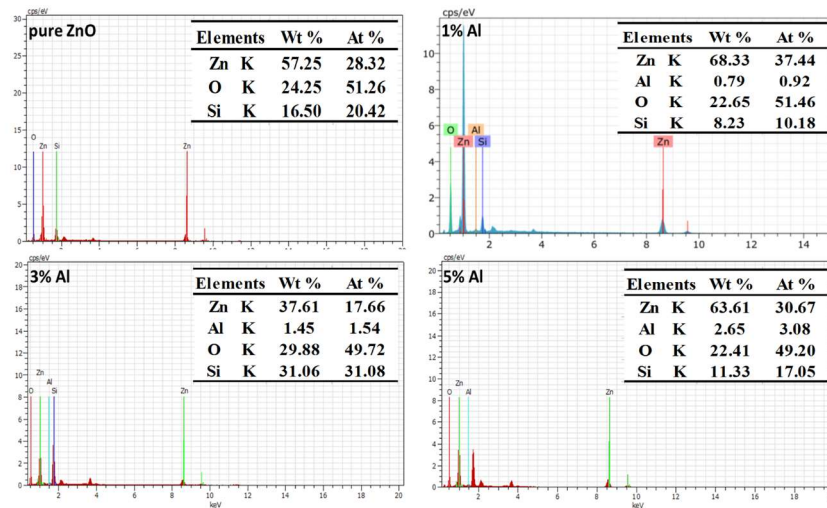


Fig.-5: EDS Images

### Optical Properties

Figure-6 shows the absorption spectra of the prepared samples. With increasing Al doping, the absorption spectrum illustrates a hyperchromic effect. The UV absorbance ranges from 300nm to 378nm on the films. The absorption peak got moved to a low energy level for ZnO thin films doped with Al, and such type of result was observed by Sandeep *et al.*<sup>22</sup> With the addition of Al, the material's optical properties improve, and the absorption spectrum edge for pure ZnO is 365.77nm and is moved to 372.17nm for ZnO doped with 5% Al. The absorption spectrum shows that 5% Al has the highest absorption. This could be because of Al doping, which alters the number of unsaturated bonds, resulting in local state divergence in the bandgap.

Figure-7 depicts the relationship among  $(h\nu)$  and  $(\alpha h\nu)^2$  of ZnO film by varying Al ratio, and acquired the bandgap by mapping the straight component of the graph is indicated by the insert. The bandgap for pure ZnO thin film is 3.15eV and bandgap for (1, 3, and 5) % Al incorporated ZnO thin films are 3.12eV, 3.10eV, and 3.06eV. The bandgap shrinks as Al concentration rises, which is interpreted by a stress relaxation mechanism. This form transition towards longer wavelengths was recorded.<sup>23</sup> This shows that fault states in the bandgap are opening, which is explained by the impurity band merging with the conduction band, causing the bandgap to diminish.

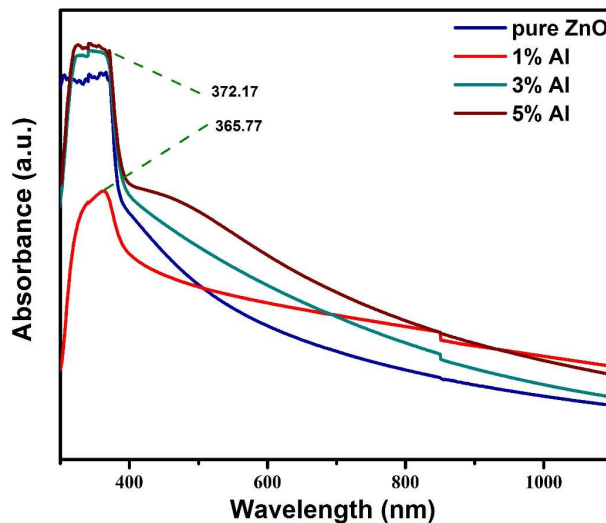


Fig.-6: Absorption spectrum

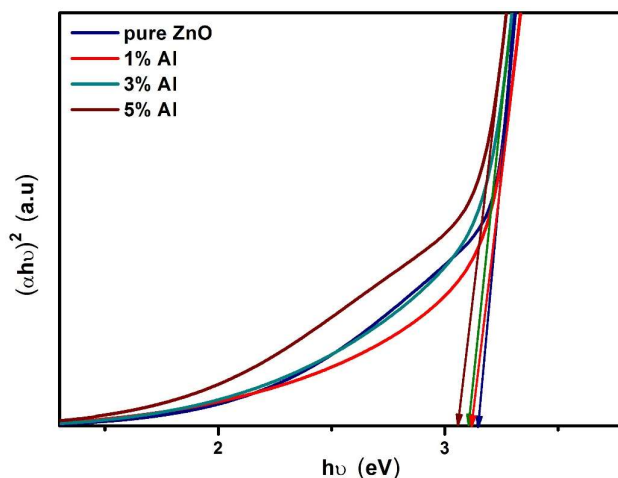


Fig.-7: Band Gap of Al incorporated ZnO and Pure ZnO Thin Films Obtained by Tauc Plot

Figure-8 depicts the photoluminescence spectrum of Al-doped ZnO with 325nm as an excitation wavelength and the image clearly shows that the prepared films produced a green emission band and a fine UV emission band. The image shows a UV peak around 381nm caused by ZnO intrinsic emission caused by free excitons recombination, as well as a deep-level emission at (450nm–550nm) caused by oxygen vacancies and zinc interstitial defect.<sup>24</sup>

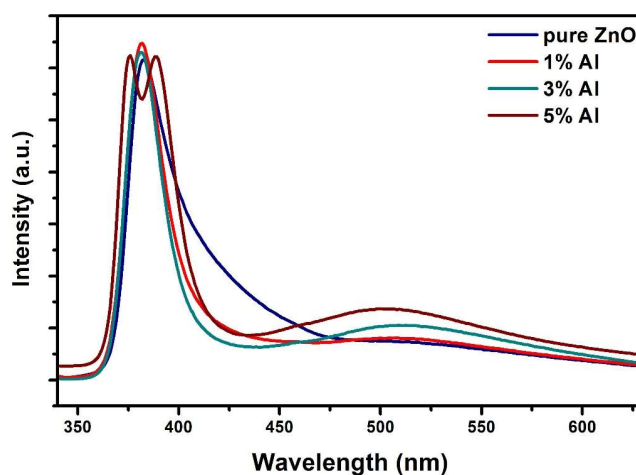


Fig.-8: PL Spectrum

### Antimicrobial Assessment

The antifungal activity is depicted in Fig.-9 for Al incorporated ZnO and pure ZnO over *Aspergillus niger*. After four days of incubation, the maximum zone of inhibition for pure ZnO is 18mm and for (1, 3, and 5)% Al content the maximum inhibition zone was 10mm, 10mm, and 17mm. Pure and Al incorporated ZnO exhibits good antifungal properties. The ZnO nanoparticles stop the *Aspergillus niger* from growing by interfering with cellular function, causing fungal hyphae to distort.<sup>25</sup> The generation of reactive oxygen species leads to a rise in cell membrane permeability, which allows for cell death.

Antibacterial action of Al incorporated ZnO and pure ZnO is represented in Fig.10. The Al incorporated ZnO produced better results compared to the pure ZnO. In *E.coli*, the maximum zone of inhibition for 5% Al-doped ZnO is about 25 mm, while with *S.aureus*, 3% Al content has a maximum inhibition zone of around 21mm. The reason for this is the strong adherence of the ZnO components with the exterior membrane of the bacteria and then, the ZnO nanoparticles have released oxygen species inside bacteria, suppressing cell growth, resulting in cell alterations and leakage, and leading to cell death. The inhibition zone demonstrates how the biocidal action of Aluminum doped ZnO damages the exterior wall of bacteria and causes death.<sup>26</sup> Physicochemical mechanisms cause cell wall disarrangement, increased oxidative

stress, and nucleic acid damage, all of which hinder bacterial cell growth and lead to death.<sup>27</sup> On E.Coli, Al-doped zinc oxide had better antibacterial activity than other strains because of the weaker cell wall.

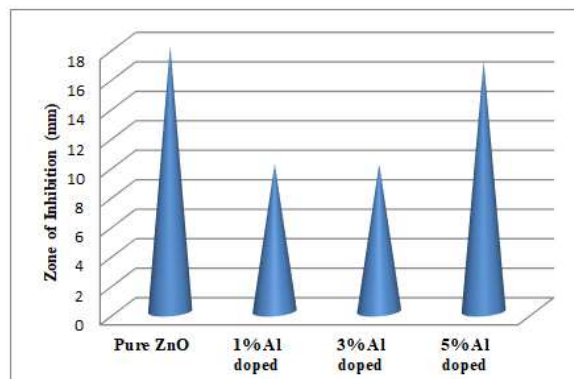


Fig.-9: Antifungal Assessment

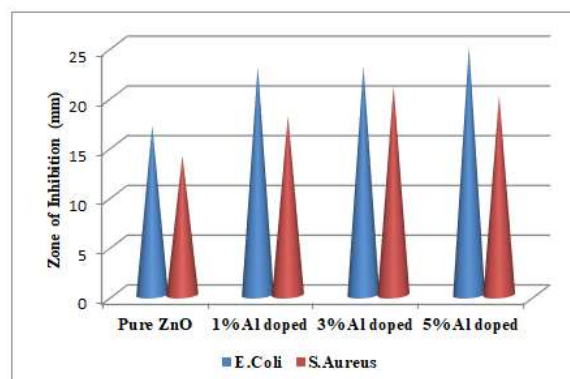


Fig.-10: Antibacterial Assessment

## CONCLUSION

The SILAR technique was used to synthesize ZnO and Al-doped ZnO thin films on glass substrates. The impact of Aluminium doped in ZnO thin films was examined. Structural findings by XRD show that all films have the same hexagonal wurtzite type crystal structure. Aluminium doping in ZnO has a significant impact on crystallite size reduction. Pure ZnO thin films have spherical morphologies, while Al-doped ZnO thin films have hexagonal oriented rod-like structures. According to an AFM investigation, RMS values increase as Al concentration rises. EDS elemental analysis confirmed the presences of Zn, O and the incorporation of Al. The optical study indicates that Al doping makes a shift in the absorption spectra to the greater wavelength side. The bandgap of ZnO was found to reduce as the Al doping ratio increased. The PL spectrum illustrates the deep level and near band emission. The Al-doped ZnO shows excellent antimicrobial activity compared to pure ZnO.

## REFERENCES

1. S. Khalili, H. M. Chenari, *Thin Solid Films*, **741**, 139031(2022), <https://doi.org/10.1016/j.tsf.2021.139031>
2. Y. Wu, F. Cao, X. Ji, *Journal of Materials Science: Materials in Electronics*, **31**, 17365(2020), <https://doi.org/10.1007/s10854-020-04292-9>
3. K. S. Siddiqi, A-ur Rahman, Tajuddin, A.Husen, *Nanoscale Research Letters*, **13**, 141(2018), <https://doi.org/10.1186/s11671-018-2532-3>
4. S. Mania, M. Cieslik, M. Konzorski, P. Swiecickowski, A. Nelson, A. Banach, R. Tylingo, *Polymers*, **12(5)**,1198(2020), <https://doi.org/10.3390/polym12051198>
5. K. Madiha, M. Abdollahi, *Iranian Journal of Pharmaceutical Research*, **20**, 216(2021), <https://dx.doi.org/10.22037/ijpr.2021.114891.15088>

6. L. Maduka, Weththimuni, D. Capsoni, M. Malagodi, M. Licchelli, *Journal of Nanomaterials*, 6715756(2019), <https://doi.org/10.1155/2019/6715756>
7. M. Rajendran, A. Arunachalam, P. Kumaresan, *Materials Research Express*, **7**, 036412(2020), <https://doi.org/10.1088/2053-1591/ab815d>
8. B. Silva, M. P. Abucafy, E. B. Manaia, J. A. Junior, B. G. Chiari-Andreo, R. Piero, L. A. Chiavacci, *International Journal of Nanomedicine*, **14**, 9395(2019), <https://doi.org/10.2147/IJN.S216204>
9. Y. Kang, F. Yu, L. Zhang, W. Wang, L. Chen, Y. Li, *Solid State Ionics*, **260**, 115544(2021), <https://doi.org/10.1016/j.ssi.2020.115544>
10. T. Shiyani, S. K. Mahapatra, I. Banerjee, *IETE Journal of Research*, 1768161(2020), <https://doi.org/10.1080/03772063.2020.1768161>
11. R. Sakhivel, A. Geetha, Ba. Anandh, A. Shankar Ganesh, *Rasayan Journal of Chemistry*, **13**,1357 (2020), <http://dx.doi.org/10.31788/RJC.2020.1335562>
12. S. U. Rahayu, Ming-Way Lee, M. N. Nasruddin, K. Sebayang, H. A. Sianturi, *Rasayan Journal of Chemistry*, **14**, 2344(2021), <http://doi.org/10.31788/RJC.2021.1446555>
13. C. E. Rojas, E. Vera, W. Aperador, *Rasayan Journal of Chemistry*, **14(01)**, 131(2021), <http://dx.doi.org/10.31788/RJC.2021.1415998>
14. J. V. Morin, E. Wahyuni, A. Suratman, A. Ashari, *Rasayan Journal of Chemistry*, **13**, 1225(2020), <http://dx.doi.org/10.31788/RJC.2020.1325720>
15. J. Bautista-Ruiz, W. Aperador, J. J. Olaya, *Rasayan Journal of Chemistry*, **11**, 597(2018), <http://dx.doi.org/10.31788/RJC.2018.1122075>
16. S. Kurtaran, *Optical Maerials*, **114**, 110908(2021), <https://doi.org/10.1016/j.optmat.2021.110908>
17. V. T. Fidal, T. S. Chandra, *Enzyme and Microbial technology*, **116**, 57(2018), <https://doi.org/10.1016/j.enzmictec.2018.05.008>
18. M. F. Malek, M. H. Mamat, M. Z. Musa, Z. Khusaimi, M. Z. Sahdan, A. B. Suriani, A. Ishak, I. Saurdi, S. A. Rahman, M. Rusop, *Journal of Alloys and Compounds*, **160**, 575(2014), <https://doi.org/10.1016/j.jallcom.2014.05.036>
19. Min-Chul Jun, Sang-Uk Park, Jung-Hyuk Koh, *Nanoscale Research Letters*, **7**, 639(2012), <https://doi.org/10.1186/1556-276X-7-639>
20. Kuang-Che Hsiao, Shih-ChiefLiao, Yi-JiaChen, *Materials Science and Engineering*, **447**, 71(2007), <https://doi.org/10.1016/j.msea.2006.10.116>
21. M. Kumar, B. Singh, P. Yadav, V. Bhatt, M. Kumar, K. Singh, A. C. Abhyankar, A. Kumar, Ju-Hyung Yun, *Ceramic International*, **43**, 3562(2017), <https://doi.org/10.1016/j.ceramint.2016.11.191>
22. K. M. Sandeep, S. Bhat, S. M. Dharmaprakash, *Optics & Laser Technology*, **102**, 147(2018), <https://doi.org/10.1016/j.optlastec.2017.12.031>
23. S. Jaballah, H. Dahman, I. Ghiloufi, G. Neri, L. E. Mir, *International Journal of Hydrogen Energy*, **45**, 34268(2020), <https://doi.org/10.1016/j.ijhydene.2020.09.053>
24. A. K. Ambedkar, M. Singh V. Kumar, V. Kumar, B. P. Singh, A. Kumar, Y. K. Gautam, *Surface and Interfaces*, **19**, 100504(2020), <https://doi.org/10.1016/j.surfin.2020.100504>
25. A. Erazo, S. A. Mosquera, J. E. Rodriguez-Paez, *Materials Chemistry and Physics*, **234**, 172(2019), <https://doi.org/10.1016/j.matchemphys.2019.05.075>
26. E. Sanchez-Lopez, D. Gomes, L. Bonilla, A. L. Lopez-Machado, R. Galindo, A. Cano, M. Espina, M. Ettcheto, A. Camins, A. M. Silva, A. Durazzo, A. Santina, M. L. Garcia, E. B. Souto, *Nanomaterials*, **10(2)**, 292(2020), <https://doi.org/10.3390/nano10020292>
27. S. X. T. Liang, L. S. Wong, Y. M. Lim, P. F. Lee, S. Djearmane, *South African Journal of Chemical Engineering*, **34**, 63(2020), <https://doi.org/10.1016/j.sajce.2020.05.009>

[RJC-6626/2021]